ELSEVIER

NeuroImage

www.elsevier.com/locate/ynimg
NeuroImage 25 (2005) 1205–1213

Diffusion MR imaging characteristics of the developing primate brain

Christopher D. Kroenke,[a] G. Larry Bretthorst,[b] Terrie E. Inder,[c] and Jeffrey J. Neil[a,d,*]

[a]*Department of Radiology, Washington University School of Medicine, St. Louis, MO 63110, USA*
[b]*Department of Chemistry, Washington University, St. Louis, MO 63130, USA*
[c]*Neonatal Neurology, Royal Women's and Royal Children's Hospitals; Murdoch Children's Research Institute, Melbourne, Australia*
[d]*Department of Pediatric Neurology, Washington University School of Medicine, St. Louis, MO 63110, USA*

Received 10 September 2004; revised 16 December 2004; accepted 17 December 2004
Available online 25 February 2005

Diffusion-based magnetic resonance imaging holds the potential to non-invasively demonstrate cellular-scale structural properties of brain. This method was applied to fixed baboon brains ranging from 90 to 185 days gestational age to characterize the changes in diffusion properties associated with brain development. Within each image voxel, a probability-theory-based approach was employed to choose, from a group of analytic equations, the one that best expressed water displacements. The resulting expressions contain eight or fewer adjustable parameters, indicating that relatively simple expressions are sufficient to obtain a complete description of the diffusion MRI signal in developing brain. The measured diffusion parameters changed systematically with gestational age, reflecting the rich underlying microstructural changes that take place during this developmental period. These changes closely parallel those of live, developing human brain. The information obtained from this primate model of cerebral microstructure is directly applicable to studies of human development.

Keywords: Magnetic resonance imaging; Diffusion anisotropy; Baboon brains; Brain development

Introduction

Magnetic resonance imaging (MRI) is increasingly utilized in human and animal studies to provide information relating to cerebral injury and development in the newborn. Diffusion MRI, in particular, is being applied to assess brain development (Huppi et al., 1998; Neil et al., 2002; Partridge et al., 2004; Rutherford et al., 2004). Diffusion MRI provides information about the directional dependence of water displacements due to diffusion. This, in turn, reflects underlying tissue microstructure. In white matter, for example, water moving parallel to myelinated fibers can move within or between myelin layers, without crossing membranes. Water moving orthogonal to fibers, on the other hand, must either cross myelin layers or go around them. As a result, water displacements are smaller when measured orthogonal to myelinated fibers than when measured parallel to them. Thus, water diffusion in myelinated white matter is anisotropic. The regional changes in diffusion anisotropy within the developing white matter of the newborn brain have been well appreciated for some time (Huppi et al., 1998; Neil et al., 1998).

Diffusion anisotropy has also been described within cerebral cortical gray matter in the developing human brain. Anisotropy is high early in development, with the preferred displacement direction oriented radially with respect to the cortical surface (Maas et al., 2004; Mori et al., 2001; Neil et al., 1998). This has been attributed to the orientation of radial glial fibers and the apical dendrites of pyramidal cells. As the brain matures, the magnitude of cortical diffusion anisotropy decreases (McKinstry et al., 2002; Mori et al., 2001), reflecting a loss in orientational coherence of cortical structures that restrict diffusion. This may be due to the elaboration of pyramidal cell basal dendrites, addition of interneurons, and/or development of thalamocortical afferent fibers. Thus, diffusion anisotropy has the potential to provide information about microstructural changes associated with both gray and white matter development.

One potential clinical application of diffusion MR imaging relates to the evaluation of the microstructural characteristics of the brain in prematurely born infants. Between 5 and 15% of prematurely born children develop cerebral palsy, and 30 to 50% will have impaired academic achievement and/or behavioral disorders requiring additional educational resources (Hack and Fanaroff, 1999; Hack et al., 2002; Saigal et al., 1991; Whitaker et al., 1997; Whitfield et al., 1997). The nature of the cerebral lesion predisposing the prematurely born child to such long-term neurodevelopmental difficulties is not well understood, as the association between abnormalities detected on conventional MRI studies and cognitive neurodevelopmental outcome is relatively weak (Cooke and Abernethy, 1999). One potential explanation for these findings is that there are subtle alterations in cerebral

* Corresponding author. Pediatric Neurology, St. Louis Children's Hospital, One Children's Place, St. Louis, MO 63110, USA. Fax: +1 314 362 0526.
E-mail address: neil@wustl.edu (J.J. Neil).
Available online on ScienceDirect (www.sciencedirect.com).

1053-8119/$ - see front matter © 2004 Elsevier Inc. All rights reserved.
doi:10.1016/j.neuroimage.2004.12.045

structure that are not detectable by conventional MRI methods. More sensitive MRI analysis techniques, such as quantitative volumetric studies, have shown a relationship between changes in MR-measured cerebral volumes and both premature birth (Inder et al., 1999) and subsequent cognitive outcome (Abernethy et al., 2002; Nosarti et al., 2002; Peterson et al., 2000). Diffusion MR imaging may complement such macrostructural volumetric data by reflecting alterations in the microstructural development of gray and white matter in these infants, further enhancing our understanding of the anatomic substrate for the increased susceptibility for neurodevelopmental difficulties in this high risk population. To make effective use of this methodology, it is important to have detailed information about diffusion characteristics of normal developing brain. In this study, we have assessed diffusion in baboon brain.

Consensus has not yet been reached regarding the optimally informative model of water displacements in the developing brain. The most commonly adopted mathematical formalism used to express diffusion anisotropy in brain is the diffusion tensor imaging (DTI) model (Basser et al., 1994). Other expressions, such as a sum of diffusion tensors (Clark et al., 2002; Maier et al., 2004a,b), a spherical harmonic expansion of the diffusion profile (Alexander et al., 2002; Frank, 2002; Zhan et al., 2003), a function possessing higher moments than the DTI model function (e.g., kurtosis) (Liu et al., 2004; Ozarslan and Mareci, 2003), and methods for expressing diffusive displacement without reference to simplifying models (Tuch et al., 2002, 2003) have been proposed. We have found that water diffusion within fixed baboon brain may be modeled with high fidelity by selecting a single model from a series of expressions possessing varying degrees of radial symmetry on a voxel-by-voxel basis, provided that a constant term is added to the expression for the MR signal (see Appendix A). The degree of radial symmetry observed within each imaging voxel is itself an important parameter, both as a source of contrast in images, and for guiding the design of time-efficient data acquisition strategies that may be extended to human studies.

We chose to investigate diffusion in a unique non-human primate brain model because of its potentially high clinical relevance. This immature baboon model was developed in the 1990s to study the impact of respiratory therapies on lung development of prematurely born baboons (Inder et al., 2003). Prematurely born baboon infants are nursed in a neonatal intensive care unit with therapeutic intervention highly similar to that of human infants, apart from randomized respiratory interventions. At sacrifice, the brains of the animals are fixed in 10% formalin and then studied with both MRI and histopathology techniques. While a variety of animal models have been used for evaluation of brain injury in premature infants, this non-human primate model has the advantage of more closely resembling the sequence of human cerebral development. In addition, the baboon cortex shares similarity in functional organization, laminar structure, and sulcal development to that of humans.

In this study, we have evaluated brains from control animals that were sacrificed immediately after delivery. This was done to characterize the water diffusion properties of normal developing baboon brain between 90 days (18–20 weeks human gestation) and 185 days (3–4 months human age). These data not only serve as a baseline for this animal model, but also shed light on the development of the primate brain, with direct relevance to the premature human infant.

Materials and methods

All animal husbandry, handling, and procedures were performed at the Southwest Foundation for Biomedical Research, San Antonio, Texas. Animal handling and ethics were approved to conform to American Association for Accreditation of Laboratory Animal Care (AAALAC) guidelines.

Premature baboons (*Papio* sp.) were delivered by hysterotomy under general anesthesia at 90, 125, 146, 160, and 185 days. They were euthanized immediately with sodium pentobarbitone (130 mg/kg i.v.). Brains were removed at post-mortem and immersed in 10% formalin fixation solution within 10 min following sacrifice. They were then shipped to Washington University in St. Louis for MR imaging.

Quadrature rf coils of Litz design (Doty et al., 1999) (Doty Scientific, Columbia, SC), matched in size to the brains under study, were used for RF transmission and reception. Brains from 90 and 125 days gestation were placed within a 4.5-cm diameter cylindrical container filled with 10% formalin, which in turn was placed within a 5-cm diameter rf coil. The larger brains (146 days to term) were sealed within plastic bags containing 10% formalin. To minimize magnetic susceptibility gradients originating from the irregularly-shaped samples, the bags were placed within 6.8-cm diameter cylindrical containers filled with Krytox, a perfluorinated liquid (DuPont, Deepwater, NJ). The apparatus was placed within a 7-cm diameter rf coil.

Coronal, diffusion-weighted images were acquired at approximately 40% of the anterior–posterior brain length posterior to the anterior pole. This slice is anterior to the junction of the central sulcus and the interhemispheric fissure. It contains the developing motor cortex and descending white matter fibers of the anterior limb of the internal capsule. Imaging was performed on a 4.7-T small animal imaging system consisting of an Oxford Instruments (Oxford, UK) magnet and a Varian NMR Systems (Palo Alto, CA) console using a spin-echo pulse sequence. In-plane resolution was 0.3×0.3 mm^2 and slice thickness 0.45 mm (90 day brain), or 0.4×0.4 mm^2 and slice thickness 0.6 mm (125 day to term brains). The TR was 1.3 s and TE was 67 ms for all brains. The voxel-wise signal-to-noise ratio obtained in the absence of diffusion-sensitizing gradients (the $S(0)$ data point) was 31, 40, 55, 54, and 55 for the 90, 125, 146, 160, and 185 day gestational aged brains, respectively. Forty-five diffusion-weighted images of each brain were acquired using differing pulsed magnetic field gradient strengths along the x-, y-, and z-axes. Total image acquisition time varied from 16 to 24 h. Each of the 45 diffusion-sensitizing gradient configurations employed unique directions and magnitudes (i.e., the b values). The gradient magnitudes ranged from 0 to 40 G/cm in uniform steps, resulting in b values ranging from 0 to 13.8 ms/μm^2. Gradient directions were set using a random number generator that is uniform over the two polar angles in spherical coordinates. Due to the large number of diffusion directions evaluated, this sampling scheme was found to provide precise, rotationally-invariant parameter estimates when evaluated using simulated data (data not shown). For example, comparisons of the random direction sampling scheme with a 45 direction scheme based on icosahedral sampling (Batchelor et al., 2003; Hasan and Narayana, 2003) yielded extremely small differences in parameter estimates from simulated data (approximately one order of magnitude less than the uncertainty in the estimates). The diffusion-sensitizing gradient pulse length, δ, was 5 ms. The inter-pulse spacing, Δ, was 50 ms. Phase-sensitive images were

calculated for each diffusion setting so that background experimental noise was Gaussian, with a mean value of zero. The MR signals were purely absorptive (no imaginary component) for all diffusion settings.

Bayesian probability theory was used both for model selection and parameter estimation. Model selection was performed on a voxel-by-voxel basis using the family of models shown in Fig. 1 (see also Appendix A). Results are presented via a color-coding system in which arbitrary colors are assigned to each model. The specific colors chosen in this study derive from ten evenly spaced points spanning the "jet" colorbar in MATLAB (The MathWorks, Inc., Natick, MA), as illustrated in Fig. 1. Using this system, images of the model selection results may be displayed as color maps. The shapes shown in Fig. 1 represent contour surfaces of a single probability of displacement from the origin at a given time. These models range from no signal through full tensor plus a "constant." The Bayesian calculations exact a penalty for each adjustable parameter included in the selected model. As a result, the model selection procedure chooses the most parsimonious model for each voxel. Once the appropriate model was chosen, probability theory was used to estimate the following parameters: the major eigenvalues of the diffusion matrix **D** (λ_1, λ_2, and λ_3, see Appendix A), the average of the three eigenvalues ($\mathbf{D}_{av}$), diffusion anisotropy (A_σ), the orientation of the principal eigenvector (through the angles ϕ, θ, and ψ, see Appendix A), and the fractional value of the constant term ($C/S(0)$). The constant term can be viewed as a subpopulation of water molecules with very slow or highly restricted diffusion. In this fashion, it is similar to the "slow component" of diffusion reported for some in vivo studies (Clark and Le Bihan, 2000; Mulkern et al., 2001).

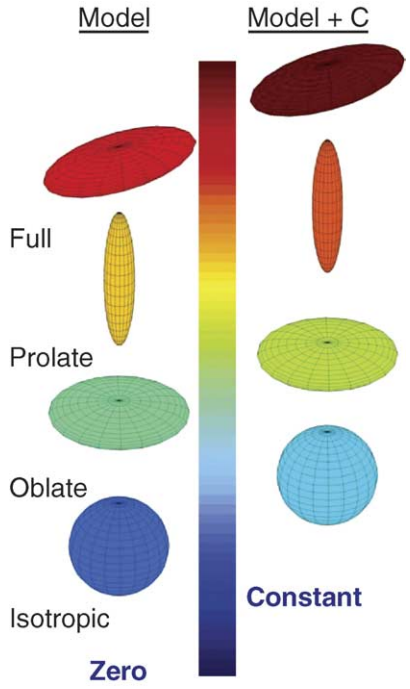

Fig. 1. A pictorial representation of the mathematical expressions used to model the diffusion MR data. Diffusion for each model is represented as an ellipsoidal surface in which the directionally-dependent diffusion coefficients (given by the eigenvalues λ_1, λ_2, and λ_3) are encoded in the excursion from the ellipsoid center. The left (model) and right (model + C) columns correspond to data modeled to a diffusion tensor with and without a constant term, respectively (see Appendix A). The "full" ellipsoids shown in the top row are centrosymmetric, and possess three unique radii corresponding to the eigenvalues $\lambda_1 > \lambda_2 > \lambda_3$. The prolate (cigar-shaped) ellipsoids shown in the second row are axisymmetric. In this case, $\lambda_1 > \lambda_2 = \lambda_3$ and the cigar has a circular cross section perpendicular to its long axis. The oblate (pancake-shaped) ellipsoids shown in the third row are also axisymmetric. In this case, $\lambda_1 = \lambda_2 > \lambda_3$, and the pancake has a circular cross section perpendicular to its short axis. For the isotropic ellipsoids, $\lambda_1 = \lambda_2 = \lambda_3$, and the shapes are spherical.

A computer program written in-house employed Markov chain Monte Carlo simulations and uninformative (uniform or broad Gaussian) prior probabilities to perform the Bayesian calculations. Details of these calculations, and how they were implemented, are explained elsewhere (Bretthorst et al., 2004). The posterior probabilities for the models shown in Fig. 1, and of the relevant parameters over specified ranges, were determined for each voxel, given the 45 MR signal intensity data values. The Bayesian analysis program output image data files, which were visualized using MATLAB software.

Results

Model selection in relation to brain or non-brain regions

The model selection results from brains of varying gestational ages are shown in Fig. 2. The regions shown include (1) the volume surrounding the formalin-bathed brain, (2) the formalin surrounding the brain, and (3) the brain. The first of these regions contains only air or perflurocarbon, and no MR signal is expected. The model selection procedure correctly assigns the "zero" model (dark blue) to the overwhelming majority of the voxels within this region, although noise contributes to other model assignments for a small fraction of these voxels. Within the formalin surrounding the brain, diffusion is expected to be isotropic and the MR diffusion signal amplitude is expected to decay to zero. In this region, the model selection procedure correctly identifies isotropic diffusion without a constant offset (dark blue) for nearly all voxels. Within the brain, the array of selected diffusion models is diverse. The resulting image of the selected models generates a recognizable representation of the brain (for example, there is contrast between cortical and non-cortical regions). This fact indicates that the voxel-wise model selections are sensitive to properties of the underlying brain microstructure. One noteworthy property of nearly all models selected within the brain, but not within the surrounding formalin, is the presence of the constant offset term.

The relationship of the brain diffusion variables to gestational age

Within the cortex, diffusion predominantly exhibits prolate symmetry (orange) from 90 days through term (Fig. 2). The model selection results are presented in terms of ellipsoid maps of diffusion at 90 and 185 days in Fig. 3. Note the radial orientation of the principal axes of the ellipsoids in cortex. While especially prominent at 90 days gestation, this pattern is still present at term. In contrast, diffusion within white matter is predominantly isotropic (powder blue) at 90 days. Between 125 and 146 days, anisotropy is increasingly detectable in most subcortical areas. By 185 days, diffusion anisotropy is characterized by oblate symmetry (lime green) at the interface between white and gray matter and by non-axially-symmetric diffusion (dark brown) in the deeper white matter (Fig. 2). At the gyral tips, the orientation of

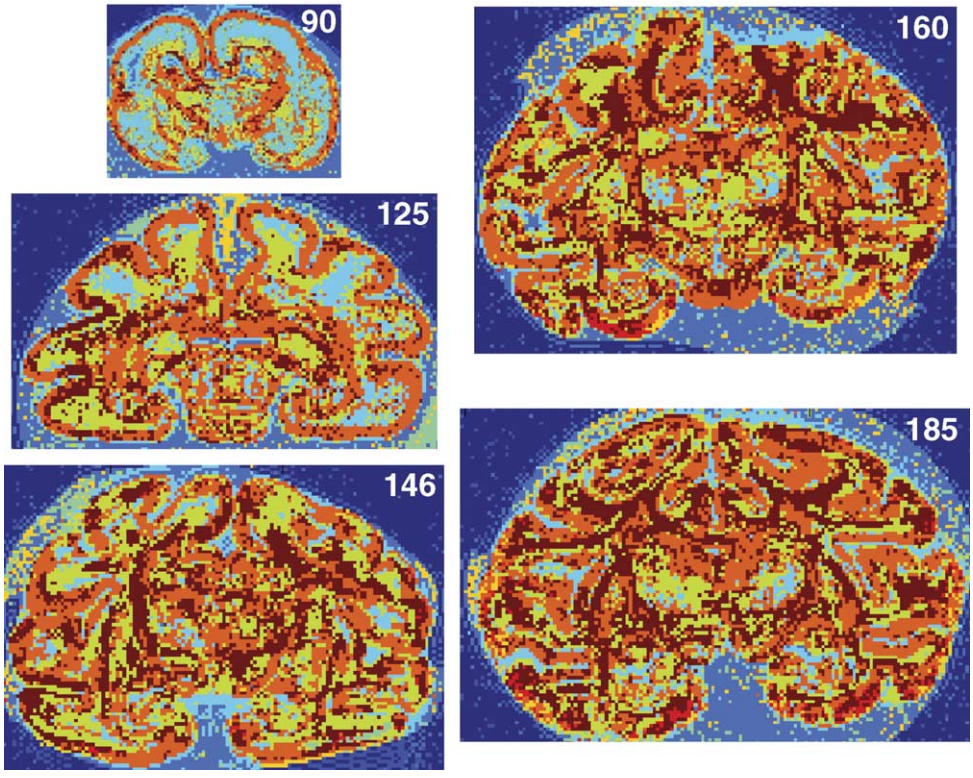

Fig. 2. Color-coded maps showing the models chosen for brains of various gestational ages, expressed in days post conception. The colors used correspond to the ellipsoid surfaces in Fig. 1. See text for details.

ellipsoids at 185 days tends to follow fiber tracts as they enter the cortex (Fig. 3).

Anisotropy and directionally-averaged diffusivity maps at various gestational ages are shown in Figs. 4 and 5, respectively. Anisotropy is prominent in cortex at 90 days. By 185 days, anisotropy is more prominent in white matter, particularly the myelinated white matter of the internal capsule. Some, although reduced, anisotropy remains within the cortex at term. There is strong gray-white contrast in $\mathbf{D}_{av}$ images from 90 to 125 days gestation, with diffusivity values higher in white matter than gray. This contrast steadily diminishes with increasing gestational age.

Comparing the A_σ and $\mathbf{D}_{av}$ data for cortex, Figs. 4 and 5 show anisotropy decreasing from 90 days gestation to term, while $\mathbf{D}_{av}$ remains constant. In terms of directionally-specific diffusivities λ_1, λ_2, and λ_3; diffusion perpendicular to the cortical surface (λ_1) decreases by 20% between 90 days and term. This is associated with an increase in diffusivity parallel to the cortical surface (λ_2 and λ_3). This combination of changes leads to a decrease in A_σ. In contrast, in the white matter, A_σ increases and $\mathbf{D}_{av}$ decreases throughout the latter half of gestation. Here, decreases in diffusivity are seen for λ_1, λ_2, and λ_3 during development. The decrease is greatest for λ_2 and λ_3, which correspond to diffusion perpendicular to the local (axon fiber) axis. This decrease is approximately 50% from 90 days to term. For λ_1, which corresponds to diffusion parallel to the local (axon fiber axis), a 10% drop is observed over the same period of time. The disproportionate decreases in directional diffusivities cause the observed increases in A_σ with gestational age.

Maps of the constant term fractional value are shown in Fig. 6. At 125 days, the constant term is largest in the ventricular and subventricular zones surrounding the lateral ventricles. Rapid cell division occurs within these regions, which collectively constitute the germinal matrix, the source of many cortical neurons (Rakic, 1995). Later in the gestational period, the fractional constant image changes to become strongly associated with areas of myelinated white matter, such as the internal capsule of the 185 day brain shown in Fig. 6.

Discussion

These diffusion MR data reveal two key observations that are of direct relevance in the study of non-human primate cerebral development. First, as described below, they assist in understanding how cellular-level tissue structure influences diffusion-based MRI contrast. Second, they demonstrate that significant changes in the diffusion characteristics of cerebral gray and white matter accompany development in this baboon model. These changes in diffusion characteristics are strikingly similar to those described in the human infant, confirming the translational utility of this model.

It is important to acknowledge that the tissue specimens used were not in vivo but rather were post-mortem and fixed in formalin. Studies have demonstrated that although $\mathbf{D}_{av}$ values are reduced by roughly a factor of three in fixed brain, diffusion anisotropy characteristics are identical for live and fixed brain (Sun et al., 2003). Thus, the results obtained in this study are relevant to studies of live subjects. The use of fixed tissue permits long MR scanning times, which translates to higher spatial resolution (<600 μm^3) as well as more detailed exploration of the spatial characteristics of diffusion (45 directionally-varying b values).

Parameters estimated in diffusion MR analyses are averages over heterogeneous microstructural regions within imaging voxels, and therefore these parameters represent statistical measures of the

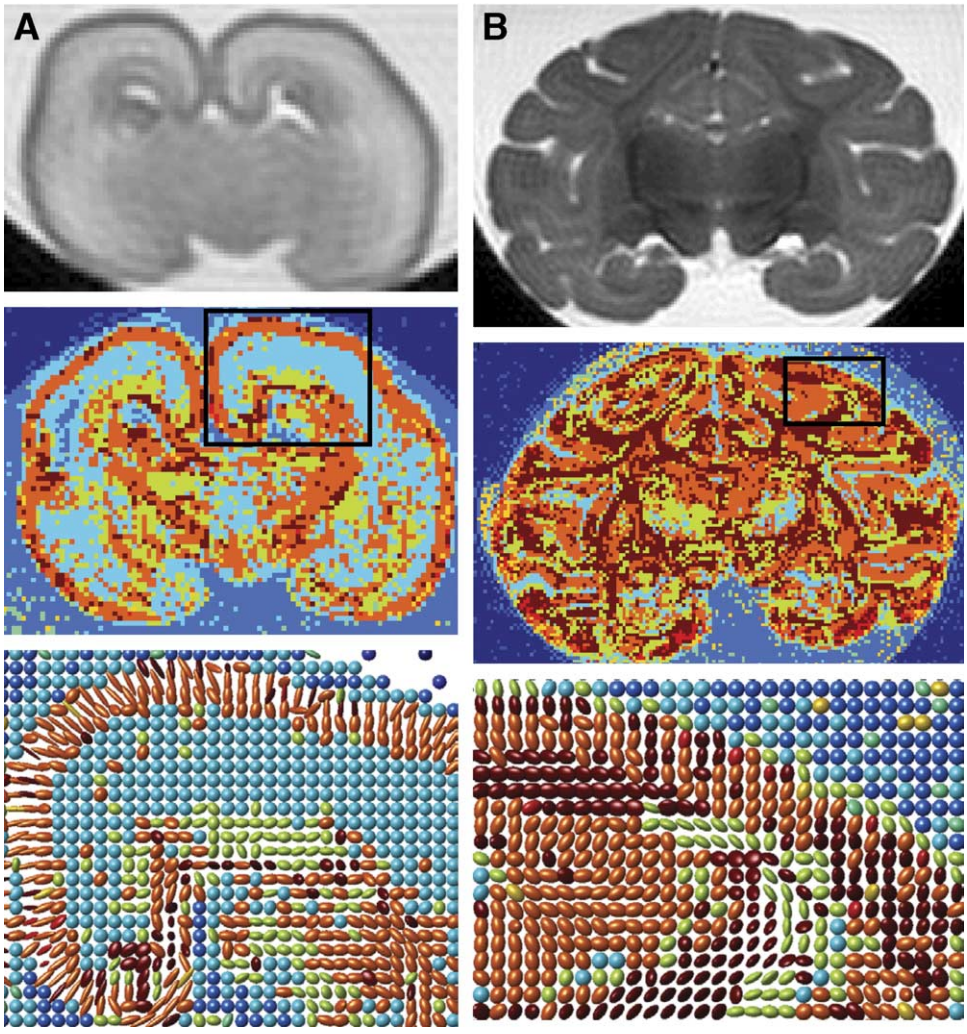

Fig. 3. Images from (A) premature (90 days) and (B) term (185 days gestation) brains. T2-weighted images are shown in the top row for reference. The middle row shows the corresponding color-coded model selection maps. The ellipsoid maps in the bottom row are taken from the boxes shown in the model selection maps. See text for details.

underlying tissue structure. The best way to convey these statistical features in terms of tissue characteristics such as cell density, type, or shape is currently an area of active investigation (Alexander et al., 2002; Clark et al., 2002; Frank, 2002; Liu et al., 2004; Maier et al., 2004a,b; Ozarslan and Mareci, 2003; Tuch et al., 2002, 2003; Zhan et al., 2003). An optimal diffusion model retains the full complement of structural information present in the data, but contains a minimal number of adjustable parameters. To ensure that the modeling procedure described in Fig. 1 provides a faithful representation of the experimental data, residual differences between the calculated diffusion MRI signal decay and the experimental data were calculated for the 45 data points within each image voxel (manuscript in preparation, and see Kroenke et al., 2004). The standard deviations in the residuals for each voxel were found to be equal to the standard deviation in the experimental noise observed in image regions containing no signal. This indicates that the adopted model selection procedure represents the data to within experimental uncertainty, and that further elaboration of the model by including additional adjustable parameters is unwarranted because it will result in fitting experimental noise. The Fig. 1 modeling procedure is relatively simple, requiring no more than eight adjustable parameters per imaging voxel, yet it clearly distinguishes cerebral structures (such as cortical from non-cortical regions) and allows structural changes to be tracked throughout development.

One unique feature of the diffusion model employed here is the addition of a constant term to the signal decay expression. Detailed MR studies of living human brain have lead to the observation that water diffusion is multi-modal, exhibiting "fast" and "slow" components (Clark and Le Bihan, 2000; Mulkern et al., 1999, 2001), with the majority of water molecules belonging to the "fast" subpopulation. In contrast, under more typical experimental or clinical conditions, the b value sampling is limited to 1.0 ms/μm^2 or less, and parameter estimates primarily reflect the majority "fast" component. In modeling diffusion within fixed baboon brain, it has been found that the multi-modal character may be concisely modeled by adding a single constant offset parameter to the diffusion expression (see Appendix A and Kroenke et al., 2004). Thus, the remaining diffusion parameter values correspond to what has been reported as the "fast" component of diffusion. In humans, the fraction of the "slow" component in myelinated white matter is found to be higher (~35%) than in gray matter (~27%) (Clark and

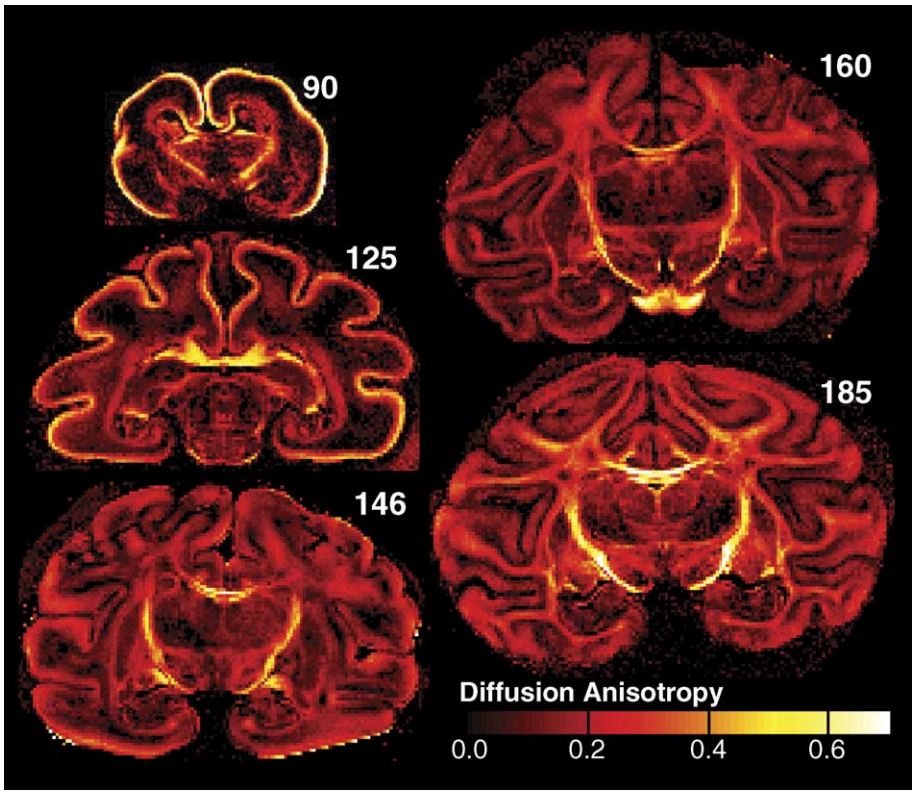

Fig. 4. Diffusion anisotropy maps at various gestational ages. Image color intensity corresponds to values for A_σ. See text for details.

Le Bihan, 2000; Mulkern et al., 1999, 2001). The data in Fig. 6 parallel these findings, with fractional constant values within white matter reaching 15% and gray matter being substantially lower, at 5% or less.

The presence of a relatively large "slow" component within white matter identified in humans suggests a relationship to water molecules trapped within the lipid layers of myelin. The pattern of the fractional constant observed in the term baboon brain further

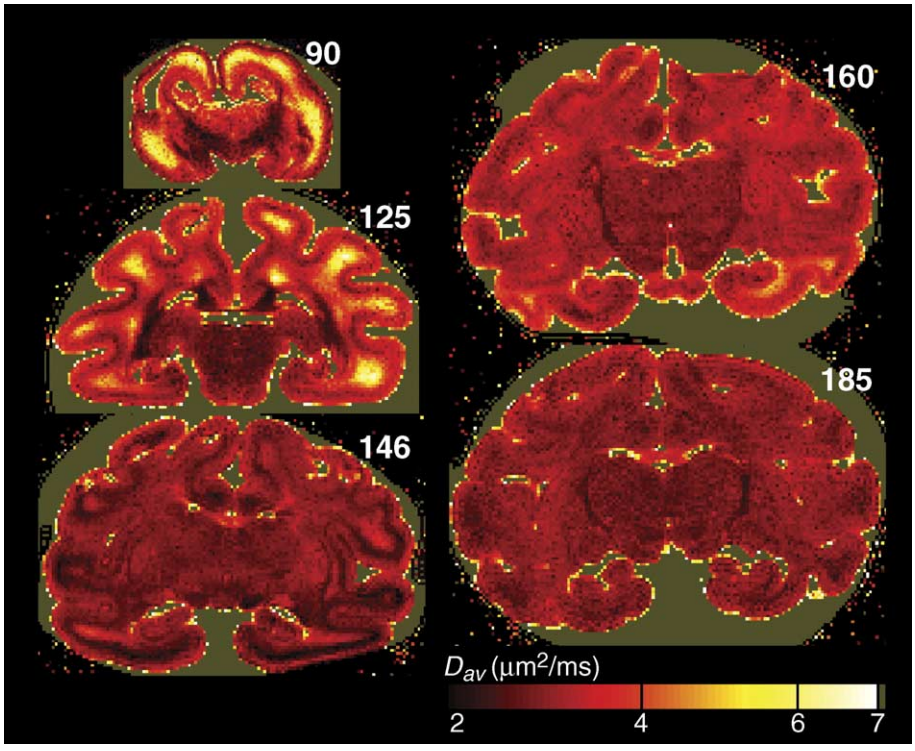

Fig. 5. $\mathbf{D}_{av}$ maps at various gestational ages. Image color intensity corresponds to values for $\mathbf{D}_{av}$. See text for details.

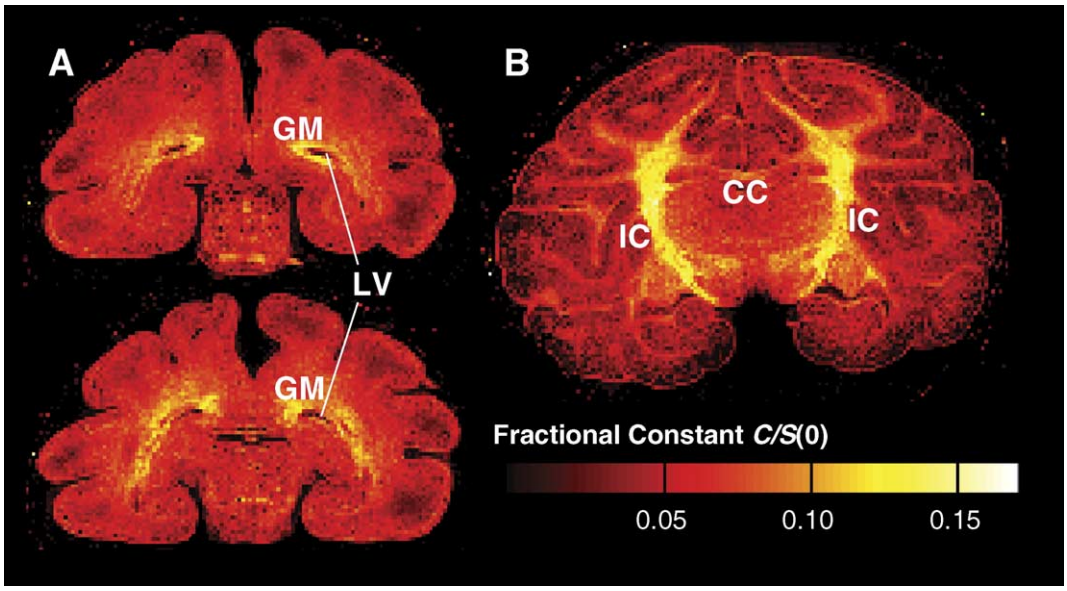

Fig. 6. Images of the fractional constant value, $C/S(0)$, at (A) 125 days and (B) 185 days gestation. Two coronal images along the anterior/posterior axis are shown of the 125 day brain to highlight the presence of high fractional constant within the germinal matrix (GM) surrounding the lateral ventricles (LV). In the term brain, the high fractional constant is present within the internal capsule (IC) but not in the corpus callosum (CC).

buttresses this hypothesis by exhibiting high values in structures that become myelinated earlier, such as the internal capsule (Kinney et al., 1988), and lower fractional values within structures that are later to myelinate, such as the corpus callosum (Kinney et al., 1988). It is interesting that the constant term also has a relatively high fractional value in the germinal matrix of 125-day brains. This may be related to the unique lipid composition and/or histologic features of this highly cellular, rapidly-dividing brain region. To investigate the possibility that the constant term directly arises from imaging ^{1}H signal of lipid, localized spectra of the term brain internal capsule were acquired (data not shown). No unique spectral characteristics of the high fractional constant region could be identified, and thus it is unlikely that the slow component represents lipid MR signal.

The trends in the other diffusion parameters throughout the latter half of gestation match those previously described in studies of live premature human infants. One advantage of the baboon model is the high precision achievable in gestational staging. Knowledge of gestational age to within 1 day has yielded very little inter-animal variability among age-matched controls (data not shown). Two or more brains have been investigated at all gestational ages, and in all cases the inter-animal variability is less than inter-age-group variability (data not shown). The diminishing gray–white contrast of $\mathbf{D}_{\mathrm{av}}$ maps with increasing gestational age is identical to the observations for the human infant (Huppi et al., 1998; Neil et al., 1998). Furthermore, the principal axis of diffusion in cerebral cortex is oriented radially, as has been shown for developing human cortex (McKinstry et al., 2002). One notable difference between the human studies and the baboon studies described here is that, for the baboon brain, A_σ values within the cortex remain non-zero, even at term (equivalent to age 3–4 months for human). Our previous report from human infants indicated that A_σ values reach zero at approximately 35 weeks gestational age (McKinstry et al., 2002). This discrepancy is likely related to partial volume averaging and signal-to-noise ratio. For the baboon study, the higher spatial resolution and signal-to-noise ratio allowed detection of lower (but nonzero) A_σ values for cerebral cortex than have been detectable in corresponding human studies. Despite this minor difference in cortical diffusion anisotropy, the consistency between the human and baboon data suggests that the fixed baboon model provides an informative model of human development.

Changes in MR-measured anisotropy within the cortex echo the microstructural changes taking place during development, and are consistent with diffusion MR-based findings in the developing mouse brain (Mori et al., 2001; Zhang et al., 2003). At the earliest developmental stages examined here (90 days gestation), ontogenic columns are already formed and are highly structured. Diffusion at this gestational age exhibits prolate symmetry and high anisotropy. This likely reflects the radial orientation of apical dendrites of pyramidal cells and radial glial fibers. During cortical maturation, pyramidal cells elaborate basal dendrites, radial glia are reduced in number, thalamocortical afferents are added, and interneurons increase in number. These changes would be expected to hinder water diffusion orthogonal to the cortical surface. The finding that values for diffusion along the principal axis of diffusion (λ_1, which is oriented radially in cortex, or orthogonal to the cortical surface) decrease with increasing gestational age is consistent with this explanation. While the prolate symmetry and radial orientation of diffusion ellipsoids is preserved, values for A_σ become smaller as a result of the reduction in λ_1 and associated diffusivity increases in the remaining directions. It is worth noting that these anisotropy features are still present at term. It may be possible to use MR diffusion techniques to evaluate the integrity of cerebral cortex in premature human infants, both early in their hospital course and/or at term equivalent, by assessing cortical anisotropy.

Diffusion anisotropy is also useful for assessing cerebral white matter development. In human infants, diffusion anisotropy is typically zero or low in regions containing unmyelinated axons, particularly during early development (Neil et al., 1998). Subsequent increases in diffusion anisotropy accompany entry of axonal fibers into a “premyelinating state” (Neil et al., 1998;

Wimberger et al., 1995), before the development of myelin layers. Further increases in anisotropy occur upon myelination (Huppi et al., 1998; Neil et al., 1998). Observations in the baboon are consistent with these findings. Diffusion is isotropic within the intermediate zone separating the periventricular region from the cortex at 90 and 125 days gestation (Rakic, 1995). At 146 days, the simultaneous rise in diffusion anisotropy in the developing white matter, and drop in cortical diffusion anisotropy suggest the emergence of cortical afferent and efferent axonal connections. Diffusion anisotropy further increases within the developing white matter throughout the remainder of gestation, with the highest values observed in myelinated areas such as the corticospinal tract.

In conclusion, changes in diffusion characteristics for fixed, developing baboon brain closely mimic those found in live, developing human brain. Thus, the fixed baboon brain model has potential for determining how water diffusion characteristics of immature and injured brain relate to cellular anatomy at a level unprecedented in human studies. Our data also indicate that diffusion measurements derived from relatively sparse angular diffusion sampling schemes (which are achievable with reasonable image acquisition times using standard clinical scanners) can provide robust diffusion anisotropy characterization of both cerebral cortex and within white matter in infants. The high imaging resolution and high precision diffusion MR data obtained with the fixed tissue enabled a detailed characterization of baboon brain development. Relationships observed between diffusion model parameters and known anatomical changes suggest that diffusion MR is highly sensitive to cellular-scale tissue structure in the primate brain. Studies involving detailed correlations between diffusion parameters and histology are currently under way.

Acknowledgments

This research was supported by NIH grants NS37357, NS43010, HL52636 BPD Resource Center, and P51RR13986 for facility support; the Murdoch Children's Research Institute; and the Allen P. and Josephine B. Green fund for Pediatric Neurology.

Appendix A

Under the experimental conditions of the current study, the dependence of the MR signal intensity upon diffusion-sensitizing gradient settings deviates from the predictions of the DTI model of Basser et al. (Basser et al., 1994). The DTI model is represented by the following expression for $S(\vec{G})$, the MR signal intensity for a single voxel:

$$S(\vec{G}) = S(0)exp\left(-\kappa(\vec{G})\cdot\mathbf{D}\cdot(\vec{G})^T\right)\equiv\mathrm{DTI} \quad (1)$$

in which $\vec{G}$ is the vector describing the diffusion-sensitizing magnetic field gradient strength and direction, and $\vec{G}^T$ is its transpose. The parameter $S(0)$ is the signal amplitude for $\vec{G} = (0,0,0)$, and $\kappa = \gamma^2\delta^2\Delta$ is determined by the diffusion-sensitizing gradient length (δ) and spacing (Δ) specified above and the ^{1}H magnetogyric ratio γ, and $\mathbf{D}$ is a 3 × 3 matrix (Basser et al., 1994)

$$\mathbf{D} = \begin{pmatrix} \mathbf{D}_{xx} & \mathbf{D}_{xy} & \mathbf{D}_{xz} \\ \mathbf{D}_{yx} & \mathbf{D}_{yy} & \mathbf{D}_{yz} \\ \mathbf{D}_{zx} & \mathbf{D}_{zy} & \mathbf{D}_{zz} \end{pmatrix}. \quad (2)$$

According to the DTI formalism, $\mathbf{D}$ is symmetric ($\mathbf{D}_{ij} = \mathbf{D}_{ji}$) and can be diagonalized by a 3 × 3 rotation matrix, $\mathbf{R}$, which is a function of the three variables ϕ, θ, and ψ

$$\mathbf{D} = \mathbf{R}(\phi,\theta,\psi)\cdot\begin{pmatrix} \lambda_1 & 0 & 0 \\ 0 & \lambda_2 & 0 \\ 0 & 0 & \lambda_3 \end{pmatrix}\cdot\mathbf{R}^T(\phi,\theta,\psi), \quad (3)$$

in which λ_1, λ_2, λ_3, are real and positive. The definitions of ϕ, θ, and ψ used in this study are those given by Conturo et al. (Conturo et al., 1996).

A simple modification of the DTI expression, the addition of a constant term, C, enables the diffusion MR data to be modeled to within experimental error. The specific expression is

$$S(\vec{G}) = \mathrm{DTI} + C. \quad (4)$$

This constant term is independent of the diffusion-sensitizing gradient settings, and is physically conceivable as a subset of water molecules whose motion is highly restricted. It has further been found that, upon inclusion of the constant, the remaining $S(\vec{G})$ expression may be simplified considerably by accounting for symmetry in the $S(\vec{G})$ data values without sacrificing the fidelity of the model to the experimental data (Kroenke et al., 2004).

References

Abernethy, L.J., Palaniappan, M., Cooke, R.W., 2002. Quantitative magnetic resonance imaging of the brain in survivors of very low birth weight. Arch. Dis. Child. 87, 279–283.

Alexander, D.C., Barker, G.J., Arridge, S.R., 2002. Detection and modeling of non-Gaussian apparent diffusion coefficient profiles in human brain data. Magn. Reson. Med. 48, 331–340.

Basser, P.J., Mattiello, J., LeBihan, D., 1994. Estimation of the effective self-diffusion tensor from the NMR spin echo. J. Magn. Reson. B 103, 247–254.

Batchelor, P.G., Atkinson, D., Hill, D.L., Calamante, F., Connelly, A., 2003. Anisotropic noise propagation in diffusion tensor MRI sampling schemes. Magn. Reson. Med. 49, 1143–1151.

Bretthorst, G.L., Kroenke, C.D., Neil, J.J., 2004. Characterizing water diffusion in fixed baboon brain. In: Dose, V. (Ed.), 24th International Workshop on Bayesian Inference and Maximum Entropy Methods in Science and Engineering, Garching, Germany. American Institute of Physics, Melville, New York, pp. 3–15.

Clark, C.A., Le Bihan, D., 2000. Water diffusion compartmentation and anisotropy at high b values in the human brain. Magn. Reson. Med. 44, 852–859.

Clark, C.A., Hedehus, M., Moseley, M.E., 2002. In vivo mapping of the fast and slow diffusion tensors in human brain. Magn. Reson. Med. 47, 623–628.

Conturo, T.E., McKinstry, R.C., Akbudak, E., Robinson, B.H., 1996. Encoding of anisotropic diffusion with tetrahedral gradients: a general mathematical diffusion formalism and experimental results. Magn. Reson. Med. 35, 399–412.

Cooke, R.W., Abernethy, L.J., 1999. Cranial magnetic resonance imaging and school performance in very low birth weight infants in adolescence. Arch. Dis. Child., Fetal Neonatal Ed. 81, F116–F121.

Doty, F.D., Entzminger, G., Hauck, C.D., 1999. Error-tolerant RF litz coils for NMR/MRI. J. Magn. Reson. 140, 17–31.

Frank, L.R., 2002. Characterization of anisotropy in high angular resolution diffusion-weighted MRI. Magn. Reson. Med. 47, 1083–1099.

Hack, M., Fanaroff, A.A., 1999. Outcomes of children of extremely low birthweight and gestational age in the 1990's. Early Hum. Dev. 53, 193–218.

Hack, M., Flannery, D.J., Schluchter, M., Cartar, L., Borawski, E., Klein, N., 2002. Outcomes in young adulthood for very-low-birth-weight infants. N. Engl. J. Med. 346, 149–157.

Hasan, K.M., Narayana, P.A., 2003. Computation of the fractional anisotropy and mean diffusivity maps without tensor decoding and diagonalization: theoretical analysis and validation. Magn. Reson. Med. 50, 589–598.

Huppi, P.S., Maier, S.E., Peled, S., Zientara, G.P., Barnes, P.D., Jolesz, F.A., Volpe, J.J., 1998. Microstructural development of human newborn cerebral white matter assessed in vivo by diffusion tensor magnetic resonance imaging. Pediatr. Res. 44, 584–590.

Inder, T.E., Huppi, P.S., Warfield, S., Kikinis, R., Zientara, G.P., Barnes, P.D., Jolesz, F., Volpe, J.J., 1999. Periventricular white matter injury in the premature infant is followed by reduced cerebral cortical gray matter volume at term. Ann. Neurol. 46, 755–760.

Inder, T.E., Dieni, S., Egan, G., Tesiram, Y., Neil, J.J., Warfield, S., Yoder, B., Rees, S., 2003. A primate model of cerebral injury in the preterm infant. Pediatr. Res. 53, 25A.

Kinney, H.C., Brody, B.A., Kloman, A.S., Gilles, F.H., 1988. Sequence of central nervous system myelination in human infancy: II. Patterns of myelination in autopsied infants. J. Neuropathol. Exp. Neurol. 47, 217–234.

Kroenke, C.D., Bretthorst, G.L., Ozcan, A.O., Yoder, B., Ackerman, J.J.H., Inder, T.E., Neil, J.J., 2004. Modeling molecular diffusion in brain using Bayesian probability theory. Twelfth Annual Meeting. International Society for Magnetic Resonance in Medicine (ISMRM), Kyoto, pp. 1207.

Liu, C., Bammer, R., Acar, B., Moseley, M.E., 2004. Characterizing non-Gaussian diffusion by using generalized diffusion tensors. Magn. Reson. Med. 51, 924–937.

Maas, L.C., Mukherjee, P., Carballido-Gamio, J., Veeraraghavan, S., Miller, S.P., Partridge, S.C., Henry, R.G., Barkovich, A.J., Vigneron, D.B., 2004. Early laminar organization of the human cerebrum demonstrated with diffusion tensor imaging in extremely premature infants. NeuroImage 22, 1134–1140.

Maier, S.E., Vajapeyam, S., Mamata, H., Westin, C.F., Jolesz, F.A., Mulkern, R.V., 2004a. Biexponential diffusion tensor analysis of human brain diffusion data. Magn. Reson. Med. 51, 321–330.

Maier, S.E., Vajapeyam, S., Mamata, H., Westin, C.-F., Jolesz, F.A., Mulkern, R.V., 2004b. Biexponential diffusion tensor analysis of human brain diffusion data. Magn. Reson. Med. 51, 321–330.

McKinstry, R.C., Mathur, A., Miller, J.P., Ozcan, A.O., Snyder, A.Z., Schefft, G.L., Almli, C.R., Shiran, S.I., Conturo, T.E., Neil, J.J., 2002. Radial organization of developing human cerebral cortex revealed by non-invasive water diffusion anisotropy MRI. Cereb. Cortex 12, 1237–1243.

Mori, S., Itoh, R., Zhang, J., Kaufmann, W.E., van Zijl, P.C., Solaiyappan, M., Yarowsky, P., 2001. Diffusion tensor imaging of the developing mouse brain. Magn. Reson. Med. 46, 18–23.

Mulkern, R.V., Gudbjartsson, H., Westin, C.F., Zengingonul, H.P., Gartner, W., Guttmann, C.R., Robertson, R.L., Kyriakos, W., Schwartz, R., Holtzman, D., Jolesz, F.A., Maier, S.E., 1999. Multi-component apparent diffusion coefficients in human brain. NMR Biomed. 12, 51–62.

Mulkern, R.V., Vajapeyam, S., Robertson, R.L., Caruso, P.A., Rivkin, M.J., Maier, S.E., 2001. Biexponential apparent diffusion coefficient parametrization in adult vs newborn brain. Magn. Reson. Imaging 19, 659–668.

Neil, J.J., Shiran, S.I., McKinstry, R.C., Schefft, G.L., Snyder, A.Z., Almli, C.R., Akbudak, E., Aaronovitz, J.A., Miller, J.P., Lee, B.C.P., Conturo, T.E., 1998. Normal brain in human newborns: apparent diffusion coefficient and diffusion anisotropy measured using diffusion tensor imaging. Radiology 209, 57–66.

Neil, J.J., Miller, J.P., Mukherjee, P., Huppi, P.S., 2002. Diffusion tensor imaging of normal and injured developing human brain. NMR Biomed. 15, 543–552.

Nosarti, C., Al-Asady, M.H., Frangou, S., Stewart, A.L., Rifkin, L., Murray, R.M., 2002. Adolescents who were born very preterm have decreased brain volumes. Brain 125, 1616–1623.

Ozarslan, E., Mareci, T.H., 2003. Generalized diffusion tensor imaging and analytical relationships between diffusion tensor imaging and high angular resolution diffusion imaging. Magn. Reson. Med. 50, 955–965.

Partridge, S.C., Mukherjee, P., Henry, R.G., Miller, S.P., Berman, J.I., Jin, H., Lu, Y., Glenn, O.A., Ferriero, D.M., Barkovich, A.J., Vigneron, D.B., 2004. Diffusion tensor imaging: serial quantitation of white matter tract maturity in premature newborns. NeuroImage 22, 1302–1314.

Peterson, B.S., Vohr, B., Staib, L.H., Cannistraci, C.J., Dolberg, A., Schneider, K.C., Katz, K.H., Westerveld, M., Sparrow, S., Anderson, A.W., Duncan, C.C., Makuch, R.W., Gore, J.C., Ment, L.R., 2000. Regional brain volume abnormalities and long-term cognitive outcome in preterm infants. JAMA 284, 1939–1947.

Rakic, P., 1995. A small step for the cell, a giant leap for mankind: a hypothesis of neocortical expansion during evolution. Trends Neurosci. 18, 383–388.

Rutherford, M., Counsell, S., Allsop, J., Boardman, J., Kapellou, O., Larkman, D., Hajnal, J., Edwards, D., Cowan, F., 2004. Diffusion-weighted magnetic resonance imaging in term perinatal brain injury: a comparison with site of lesion and time from birth. Pediatrics 114, 1004–1014.

Saigal, S., Szatmari, P., Rosenbaum, P., Campbell, D., King, S., 1991. Cognitive abilities and school performance of extremely low birth weight children and matched term control children at age 8 years: a regional study. J. Pediatr. 118, 751–760.

Sun, S.W., Neil, J.J., Song, S.K., 2003. Relative indices of water diffusion anisotropy are equivalent in live and formalin-fixed mouse brains. Magn. Reson. Med. 50, 743–748.

Tuch, D.S., Reese, T.G., Wiegell, M.R., Makris, N., Belliveau, J.W., Wedeen, V.J., 2002. High angular resolution diffusion imaging reveals intravoxel white matter fiber heterogeneity. Magn. Reson. Med. 48, 577–582.

Tuch, D.S., Reese, T.G., Wiegell, M.R., Wedeen, V.J., 2003. Diffusion MRI of complex neural architecture. Neuron 40, 885–895.

Whitaker, A.H., Van Rossem, R., Feldman, J.F., Schonfeld, I.S., Pinto-Martin, J.A., Tore, C., Shaffer, D., Paneth, N., 1997. Psychiatric outcomes in low-birth-weight children at age 6 years: relation to neonatal cranial ultrasound abnormalities. Arch. Gen. Psychiatry 54, 847–856.

Whitfield, M.F., Grunau, R.V., Holsti, L., 1997. Extremely premature (< or = 800 g) schoolchildren: multiple areas of hidden disability. Arch. Dis. Child., Fetal Neonatal Ed. 77, F85–F90.

Wimberger, D.M., Roberts, T.P., Barkovich, A.J., Prayer, L.M., Moseley, M.E., Kucharczyk, J., 1995. Identification of "premyelination" by diffusion-weighted MRI. J. Comput. Assist. Tomogr. 19, 28–33.

Zhan, W., Gu, H., Xu, S., Silbersweig, D.A., Stern, E., Yang, Y., 2003. Circular spectrum mapping for intravoxel fiber structures based on high angular resolution apparent diffusion coefficients. Magn. Reson. Med. 49, 1077–1088.

Zhang, J., Richards, L.J., Yarowsky, P., Huang, H., van Zijl, P.C.M., Mori, S., 2003. Three-dimensional anatomical characterization of the developing mouse brain by diffusion tensor microimaging. NeuroImage 20, 1639–1648.